

Testing a hypothesis of the ν Octantis planetary system

Mariusz Słonina, Krzysztof Goździewski, Cezary Migaszewski & Anna Rozenkiewicz

Nicolaus Copernicus University, Centre for Astronomy, Gagarin Str. 11, PL-87-100 Toruń, Poland

3 March 2022

ABSTRACT

We investigate the orbital stability of a putative Jovian planet reported by Ramm et. al in a compact binary ν Octantis. Our numerical study makes use of a new computational Message Passing Interface (MPI) framework Mechanic which we developed to run massive numerical experiments on CPU clusters. The code is illustrated on a model Hamiltonian introduced by Froeschlé et al. We confirm that the ν Octantis planet could reside in a retrograde orbit, according with a hypothesis of Eberle & Cuntz. It may be present in a zone of stable motions which has a structure of the Arnold web formed due to overlapping of low-order mean motion resonances and their sub-resonances. We also re-analyzed the available radial velocity data in terms of self-consistent Newtonian N -body model. We found stable best-fit solutions that obey the observational constraints. They correspond to retrograde, strictly anti-aligned orbits of the binary and the planet. However, these solutions are confined in very small stable regions of the phase space. The presence of a real planet in the system is still questionable, because its formation would be hindered by strong dynamical perturbations.

Key words: N -body problem, numerical methods, binaries

1 INTRODUCTION

The ν Octantis is a single-line spectroscopic binary composed of the ν Oct A K1 III giant primary ($1.4 \pm 0.3 M_{\odot}$) and an unseen red dwarf secondary ν Oct B, K7-M1 V ($0.5 \pm 0.1 M_{\odot}$) separated by $\sim 2.55 \pm 0.13$ au. The orbital period is $P_{\text{bin}} = 1050.11 \pm 0.13$ days and eccentricity $e_b = 0.2358 \pm 0.0003$ (Ramm et al. 2009). Already Colacevich (1935) collected 11 radial velocities (RVs) of the primary, and Alden (1939) determined Keplerian elements of astrometric orbit. Remarkably, the inclination $i_{\text{bin}} = 71^\circ$ is recently known with an error less than 1° on the basis of Hipparchos astrometry and 223 precision RVs collected by Ramm et al. (2009). These authors discovered residual variability of the RVs $\sim 200 \text{ ms}^{-1}$ and explained it by an S-type (Dvorak 1984) Jovian planet ν Oct Ab having mass $m_p \sin i_p = 2.5 m_{\text{Jup}}$ in an orbit of the semi-major axis $a_p = 1.2 \pm 0.1$ au and eccentricity $e_p = 0.123 \pm 0.037$.

The announced planet is quite unusual, because the derived semi-major axis implies its orbit in the middle between massive primary and the secondary. The formation of such a planet in a compact binary can be hardly explained (e.g., Kley 2010). Moreover, analytic or general stability criteria formulated for the three-body problem or for the restricted three-body problem, like the Hill stability criterion, the results of Holman & Wiegert (1999), or the resonance-overlap criterion by Wisdom (1983) are violated. According with the determination of stability limits in binaries (Holman & Wiegert 1999), a coplanar, prograde planetary configuration might be stable only up to astrometric distance ~ 0.64 au (Ramm et al. 2009). Indeed, Eberle & Cuntz (2010) found that the Keplerian best-fit model in the discovery paper is strongly unstable in just 1–10 binary periods time-scale. This contradicts the planetary

hypothesis, although the discovery paper excludes non-planetary sources of the observed signal, like stellar spots or pulsations.

There are possible alternate explanations of the observed RVs variability and of the apparent paradox of strongly unstable system. The residual, unexplained RV signal can be a result of stellar chromospheric activity, a different number of planetary companions, systematic errors of the observations, including instrumental instabilities and non-Gaussian uncertainties, e.g., the red noise (Baluev 2011), or quite a different orbital model than the configuration in the discovery paper. Indeed, Morais & Correia (2012) consider a hierarchical triple system with an unseen binary in the place of secondary ν Oct B. Such an orbital setup forces a precession of the primary orbit around the barycentre of the inner binary and it could mimic the RV variations attributed to the putative planet.

Earlier, Eberle & Cuntz (2010) found that a *retrograde* orbit of the planet lies in much wider stable zone than in the direct configuration. This has been confirmed in their new paper (Quarles et al. 2012), which regards an extended set of tested orbital configurations. However, the analysis of the RVs done in the discovery paper does not seem strictly consistent with the dynamical character of the system. The mass of the secondary may be almost a half of the primary mass, hence the relatively wide planetary orbit is strongly perturbed. In the ν Oct system, the perturbation parameter (mass ratio of the secondary and the primary) can be as large as ~ 0.3 . Furthermore, it was assumed that the whole system is co-planar, no matter if the planetary orbit is prograde or retrograde. However, non-planar orbits in compact binaries may likely appear due to violent post-formation scenarios, like the planet–planet scattering (e.g., Adams & Laughlin 2003). This might imply highly inclined configurations in which the dynamics are much more complex than

in the coplanar case (see, e.g., Migaszewski & Goździewski 2011). The dynamical simulations done by Eberle & Cuntz (2010) concern initially aligned orbits and Quarles et al. (2012) consider a number of particular, equidistant relative orbital phases. The alignment of apsidal lines may maximize the probability of stable configurations but it does not necessarily reproduce the observed reflex motion of the primary. The phase space of mutually interacting planets has a non-continuous structure w.r.t. the dynamical stability. Therefore, the relative orbital phases should not be fixed or selected *a priori*, if the tested configuration is supposed to be consistent with the observations.

In this work, we aim to verify and improve the kinematic (Keplerian) model of the ν Oct planetary system by searching for the best-fit configurations in terms of self-consistent dynamical, N -body model (e.g., Goździewski et al. 2008, and references therein). To resolve the fine structure of the phase space and to investigate the dynamics and long-term stability, we apply the fast-indicator MEGNO (Cincotta et al. 2003) adapted to our new multi-CPU computing environment *Mechanic*. In this paper, we demonstrate its non-trivial application.

The paper is structured as follows. After this introduction, in Section 2, the numerical setup is described, that further refers to technical details given in the Appendix. In Sect. 3 we recall a simple Hamiltonian model analysed by Froeschlé et al. (2000), and we focus at a dynamical feature called the Arnold web. This part also illustrates the basics of the *Mechanic* environment on explicit example code. Section 4 is devoted to the dynamical analysis of the orbital solution proposed in (Eberle & Cuntz 2010). We attempt to visualize and identify extremely complex resonant structures in the vicinity of presumable planetary configuration. Finally, in Section 5, we show that stable, retrograde orbits strictly consistent with the RV observations may be found with the help of our GAMP code (Goździewski et al. 2008). Conclusions are given in the last Section 6.

2 NUMERICAL MPI FRAMEWORK

To characterize the dynamical stability of orbital models, so called fast indicators are often used (e.g., Goździewski et al. 2008). These numerical tools make it possible to resolve efficiently whether a given solution is stable (quasi-periodic, regular) or unstable (chaotic) by following relatively short parts of the orbits. The fast indicators, like the Fast Lyapunov Indicator (FLI, Froeschlé et al. 2000), the Frequency Map Analysis (FMA, Laskar 1993; Sidlichovský & Nesvorný 1996), the Mean Exponential Growth factor of Nearby Orbits (MEGNO, Cincotta & Simó 2000; Cincotta et al. 2003; Mestre et al. 2011), the Spectral Number (SN, Michtchenko & Ferraz-Mello 2001), are well known in the theory of dynamical systems (Barrio et al. 2009). In the past decade, they were intensively adapted to the planetary dynamics (e.g., Froeschlé et al. 1997; Robutel & Laskar 2001; Goździewski et al. 2008).

A computation of a fast indicator (or any dynamical characteristic of the planetary system) relies on the numerical integration of the equations of motion with an initial condition. It can be thought as a *task* in the language of computing. When examining a large volume of orbital parameters (which may be unconstrained, as in the ν Oct case), we must perform a large set of such independent computational tasks. Their result will be called *the dynamical map* from hereafter. The dynamical maps provide a quasi-global view of the phase-space. A given characteristic of a tested orbital configuration is represented by a point (*a pixel*) of the dynamical map

(*an image*) whose coordinates axes are selected orbital parameters. They encompass possible or permitted configurations, mass ranges or other physical data.

A construction of a dynamical map in possibly large resolution demands significant CPU overhead. Hence, the computations should be distributed among possibly many CPUs. Afterwards, the results must be assembled. This may be a cumbersome job, prone to human errors. Since the computations of dynamical maps are similar to image processing, we may apply a parallelization technique based, for instance, on the Message Passing Interface (MPI) (Pacheco 1996). This approach seems very natural but it is also problem-dependent. One needs to implement the communication layer, making it possible to change initial conditions in the code, to gather and store the results, to create checkpoint files to restart broken runs. Trying to resolve such issues, we developed from scratch a new numerical framework within the MPI *task farm* model. In this paper, we present the first working implementation of this framework, which is called the *Mechanic*.

There are already available general-purpose distributed task management systems of this type, like Condor (Fields 1993), or recently announced Workqueue (Yu et al. 2010). The idea of *Mechanic* basically differs from these packages in two main aspects. The first one regards a different understanding of the computation structure. We focus on self-contained code blocks (*procedures* or *routines*), rather than self-contained, standalone *applications*. The second aspect is an unified data storage making use of the well known and universal HDF5 data format (The HDF5 Group 2012). In the *Mechanic* framework, a parallel application is understood as a *module* to the management and communication layer (*the core*). This partition is achieved through enveloping computing “scalar” routines/codes by functions of the *Mechanic* Application Programming Interface (API). The API provides a relatively simple interface to the MPI layer. The core of *Mechanic* handles the task distribution and MPI communication basically transparently for the user. Actually, it closely mimics the Unix system architecture, which is build up from the kernel, providing an interface to the hardware, and the user application layer. In such a way, the *Mechanic* API basically frees the user from a deep knowledge of the parallel programming, still making it possible to “parallelize” calculations relatively easily. More details and a practical example are described in the next Sect. 3 and in the Appendix, as well as in the documentation of the package which is freely available (see <http://git.astr1.umk.pl/projects/mechanic>).

3 HAMILTONIAN MODEL OF THE ARNOLD WEB

We found a dynamical system derived by Froeschlé et al. (2000) helpful to understand the complex dynamics of the ν Oct planetary system. This simple but nontrivial example is also useful to illustrate programming concepts behind the *Mechanic* environment.

The dynamical system is written in Hamiltonian form of

$$\mathcal{H} = \mathcal{H}_0(I_1, I_2, I_3) + \epsilon V(\phi_1, \phi_2, \phi_3), \quad (1)$$

where the Hamiltonian terms are

$$\mathcal{H}_0 = \frac{1}{2}I_1^2 + \frac{1}{2}I_2^2 + I_3, \quad (2)$$

$$\mathcal{V} = \frac{1}{\cos \phi_1 + \cos \phi_2 + \cos \phi_3 + 4}. \quad (3)$$

Actions $I_1, I_2, I_3 \in \mathbb{R}$ and angles $\phi_1, \phi_2, \phi_3 \in \mathbb{T}$ are canonically conjugated variables, and ϵ is a parameter that measures the perturbation.

tion strength. Indeed, if $\epsilon = 0$, the equations of motion of Hamiltonian \mathcal{H}_0 are trivially integrable. Because angles are cyclic in \mathcal{H}_0 , actions I_1, I_2, I_3 are constant; then the angles are linear functions of time $\phi_i = f_i t + \phi_i(0)$, where

$$f_i = \frac{\partial \mathcal{H}}{\partial I_i} \equiv \frac{\partial \mathcal{H}_0}{\partial I_i}, \quad i = 1, 2, 3.$$

The motions generated by the integrable Hamiltonian are confined to invariant tori composed of quasi-periodic solutions having the fundamental frequencies $f_1 = I_1, f_2 = I_2, f_3 = 1$. With the perturbation term $\epsilon \neq 0$, the full dynamics are non-integrable. According with the Kolmogorov-Arnold-Moser theorem (KAM, Arnold 1978), the quasi-periodic solutions persist in some volume of the phase space, provided that certain non-degeneracy conditions are fulfilled and the unperturbed tori are sufficiently non-resonant:

$$k_1 f_1 + k_2 f_2 + k_3 f_3 \neq 0, \quad k_1, k_2, k_3 \in \mathbb{Z}.$$

The KAM theorem does not apply in a neighborhood of the resonances, which are represented as lines, up to the distance of the order of $\sqrt{\epsilon} \exp(-|\mathbf{k}|)$, where $|\mathbf{k}|$ is the order of the resonance. In that zone, called *the Arnold web*, the dynamics are extremely complex.

Following Froeschlé et al. (2000), we visualize the structure of the Arnold web through applying a concept of dynamical maps. The Arnold web can be represented in two-dimensional actions plane, e.g., (I_1, I_2) , which correspond to fundamental frequencies of the unperturbed system (Froeschlé et al. 2000). To detect the regular and chaotic motions, which are expected in a non-integrable Hamiltonian system, we apply the fast indicator MEGNO. Recently, Mestre et al. (2011) showed analytically that this numerical tool brings essentially the same information as the Fast Lyapunov Indicator used by Froeschlé et al. (2000). They computed dynamical maps of the Arnold web for a few representative values of $\epsilon = 0.001, \epsilon = 0.01$ and $\epsilon = 0.04$, with the resolution of 500×500 pixels.

With the help of *Mechanic*, we attempt to illustrate the Arnold web in much larger resolutions revealing very fine details of the phase space. They appear due to resonances of large orders. It is only a matter of long enough integration time to detect all resonances, but much longer motion times than 10^3 characteristic periods ($\equiv 1$) in the original paper are required. The general-purpose integrators, like the Runge-Kutta or Bulirsch-Stoer-Gragg schemes are not accurate nor efficient enough for that purpose. These methods introduce systematic drift of the energy (or other integrals). To avoid such errors, and to solve the variational equations required to compute the MEGNO indicator, we applied the symplectic tangent map algorithm introduced by Mikkola & Innanen (1999). In the past, we used this scheme for an efficient and precision computations of MEGNO for multiple planetary systems (Goździewski et al. 2003, 2005, 2008).

The model Hamiltonian is particularly simple to illustrate the symplectic algorithm. It relies on concatenating maps $\Phi_{1,h}(\mathbf{I}, \boldsymbol{\phi})$ and $\Phi_{2,h}(\mathbf{I}, \boldsymbol{\phi})$ that solve the equations of motion derived from the unperturbed part \mathcal{H}_0 , and the perturbation alone, on the time interval $[t_0, t_0 + h]$. The solutions may be constructed if both Hamiltonian terms admit analytical solutions. This is the case. For the unperturbed term we have

$$\frac{d}{dt} \boldsymbol{\phi} = \frac{\partial \mathcal{H}_0}{\partial \mathbf{I}}, \quad \frac{d}{dt} \mathbf{I} = -\frac{\partial \mathcal{H}_0}{\partial \boldsymbol{\phi}}.$$

Then the “drift” map $\Phi_{1,h}(\mathbf{I}, \boldsymbol{\phi})$ map is the following:

$$\boldsymbol{\phi} = \boldsymbol{\omega} h + \boldsymbol{\phi}_0, \quad \mathbf{I} = \mathbf{I}_0,$$

where $\mathbf{f} = (I_1, I_2, 1)$. The equations of motion generated by the perturbation Hamiltonian $H_1 \equiv \epsilon V(\boldsymbol{\phi})$ alone are also soluble, hence we obtain the “kick” map $\Phi_{2,h}(\mathbf{I}, \boldsymbol{\phi})$:

$$\boldsymbol{\phi} = \boldsymbol{\phi}_0, \quad \mathbf{I} = \boldsymbol{\Omega} h + \mathbf{I}_0, \quad \boldsymbol{\Omega} = -\epsilon \frac{\partial V(\boldsymbol{\phi})}{\partial \boldsymbol{\phi}}.$$

A classic leap-frog concatenation of these maps

$$\Phi \equiv \Phi_{1,h/2} \odot \Phi_{2,h} \odot \Phi_{1,h/2},$$

provides a numerical integrator of the second order with local error $O(\epsilon h^2)$. However, because we deal with a small perturbation parameter, much better performance and accuracy can be obtained by applying symplectic schemes invented by Laskar & Robutel (2001). The n -th order integrator, e.g., SABA $_n$, have the truncation error $O(\epsilon^2 h^2 + \epsilon h^n)$. For small ϵ it behaves like a higher-order scheme without introducing negative sub-steps. In our computations, we used the SABA $_3$ scheme. We found that it provides an optimal performance, CPU-overhead vs. the relative error of the energy.

To compute the MEGNO, we must solve the variational equations to the equations of motion. We use the algorithm described in (Goździewski et al. 2008). The tangent map approach (Mikkola & Innanen 1999) requires to differentiate the “drift” and “kick” maps. This step is straightforward. The variations are propagated within the same symplectic scheme, as the equations of motion. Having the variational vector $\boldsymbol{\delta}$ computed at discrete times, we find temporal y and mean Y values of the MEGNO indicator at the j -th integrator step ($j = 1, 2, \dots$) in the form of (Cincotta et al. 2003; Goździewski et al. 2008):

$$Y(j) = \frac{(j-1)Y(j-1) + y(j)}{j},$$

$$y(j) = \frac{j-1}{j} y(j-1) + 2 \ln \left(\frac{\delta_j}{\delta_{j-1}} \right),$$

with initial conditions $y(0) = 0, Y(0) = 0, \delta = |\boldsymbol{\delta}|$. Following Cincotta et al. (2003), the MEGNO map obtained in this way tends asymptotically to

$$Y(j) = ahj + b,$$

where $a = 0, b \sim 2$ for quasi-periodic orbits, $a = b = 0$ for stable, periodic orbit, and $a = (1/2)\sigma, b = 0$ for chaotic orbit with the maximal Lyapunov exponent σ .

Thanks to the linearity of the tangent MEGNO map, the variational vector can be normalized, if its value grows too large for chaotic orbits. In practice, we stop the integration if MEGNO reaches a given limit ($Y = 5$ in this particular case).

Calculations of the MEGNO maps were performed with different step-sizes, $h = 0.01$ up to $h = 0.5(\sqrt{5} - 1) \sim 0.29$, and $h = 0.5$ with different choices of the initial variational vector. The step-size was controlled by examining whether the relative energy error is “flat” (Goździewski et al. 2008). Indeed, it was preserved up to 10^{-10} over the total integration times up to $T \sim 10^6$. To reveal very fine details of the Arnold web, T has to be set to such large values. Typically, we set it to $T = 10^5$, in accord with the fast convergence of MEGNO.

We prepared a simple *Mechanic* module implementing the symplectic algorithm. Its full C source code is available at the website of the project, and is described in the Appendix. Calculations were performed on the *reef* cluster at the Poznań Supercomputing Centre. We did *Mechanic* runs on up to 2048 CPU cores, to derive the MEGNO maps in the resolution 2048×2048 pixels. Depending on the characteristic period T and a number of CPU cores involved.

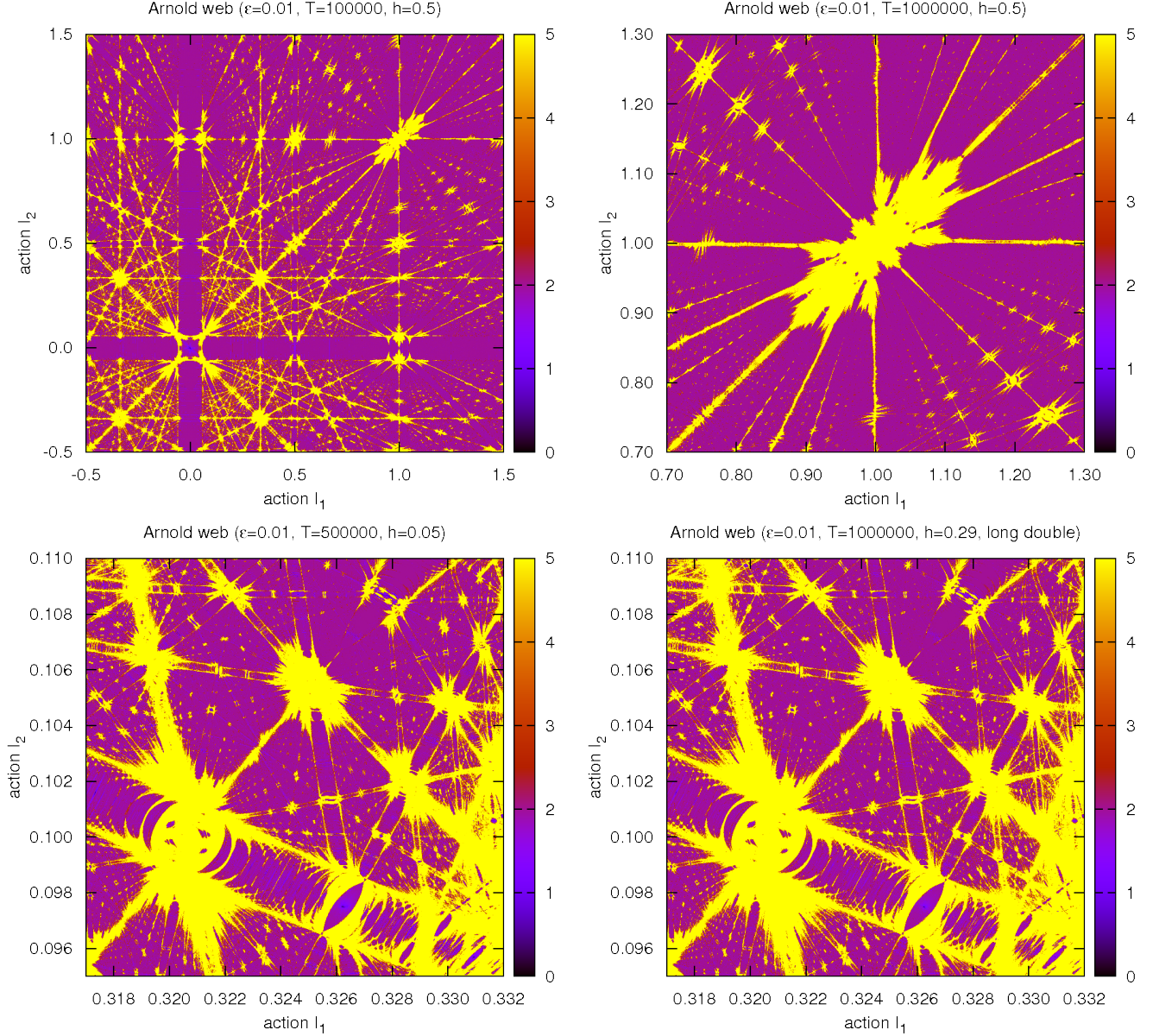


Figure 1. MEGNO dynamical maps of the test Hamiltonian Eq. 1 in the actions (I_1, I_2) -plane, corresponding to the fundamental frequencies of the unperturbed model. All panels are for $\epsilon = 0.01$. The *top left* panels is for the quasi-global view of the phase space and the *top right* panel is for a close-up around $(1,1)$. Solutions are colour-coded: stable solutions are with MEGNO ~ 2 , unstable (chaotic) with MEGNO cut-off at 5, and stable periodic orbits are marked with MEGNO ~ 0 . Original, raw resolution of the maps is 2048×2048 points. The step-size h of the symplectic SABA₃ integrator and total integration time are labeled. The *bottom row*: close-ups of MEGNO dynamical maps for $\epsilon = 0.01$, computed with the double precision (the *bottom left* panel, ~ 16 significant digits, step-size 0.05), and with the long-double precision (the *bottom right* panel, ~ 19 significant digits, step-size ~ 0.29).

Usually, we ran the computations on 128–256 CPU cores. A single run took up to a few hours.

The results for $\epsilon = 0.01$ are illustrated in Fig. 1. The top left panel is for the global view of the (I_1, I_2) -plane. The resonances are visible as straight lines. The yellow (light-gray) points encode chaotic orbits, and the purple (dark-gray) colour denotes $\langle Y \rangle \sim 2$ of stable, quasi-periodic solutions. The right panel shows a close-up of a structure in the top right corner of the global map. Both these maps were computed with relatively long step-size $h = 0.5$. We found that even such large integration steps do not introduce artificial (numerical) resonances. As an example, we selected a very small region close to the centre of the global map (the top-left

panel in Fig. 1), and we computed two maps with $h = 0.05$ over $T = 5 \times 10^5$, and with $h = 0.29$, over $T = 10^6$. In the later case, we forced the long double precision, providing about of 19 significant digits of the Intel Xeon CPUs installed in the reef cluster. Both the close-ups reveal very fine details of the phase space, and cannot be distinguished each from the other. This test assured us, that relatively large step-sizes of the order of $h \sim 10^{-1}$ is still safe, and the results are reliable.

According to Froeschlé et al. (2000), the global dynamics for $\epsilon = 0.01$ is governed by the Nekhoroshev regime. In this case, most of invariant tori in the perturbed system persist. Froeschlé et al. (2000) estimated that a transition between the Nekhoroshev regime

and the Chirikov regime, when the dynamics are driven by overlapping resonances, and a chaotic solution may wander between different resonances, takes place for $\epsilon_0 \in [0.01, 0.04]$. This phenomenon, called the Arnold diffusion, is closely related to the stability of the system. It is still not well understood and its investigations are ongoing (Cincotta 2002). Originally, the diffusion was suggested by Arnold (1964) in the three-body problem. A common understanding of the Arnold diffusion is that it may lead to significant drifts of actions along resonances. An in-depth analysis of this effect in the model Hamiltonian Eq. 1 may be found in (Lega et al. 2003, and references therein). We will show that the phase space of the ν Oct planetary system exhibits locally the structure of the Arnold web.

4 DYNAMICS OF THE ν Octantis PLANETARY SYSTEM

To resolve the paradox of the ν Octantis system instability, Eberle & Cuntz (2010) searched for stable orbits at a grid of primary mass (1.1, 1.4 and 1.7) M_\odot , three mass ratios ($\mu = 0.2593, 0.2754, 0.2908$), and 30-step initial distance ratio ρ between the planet and the secondary, $\rho \in (0.22, 0.54) \equiv (0.56, 1.38)$ au. The equations of motion were integrated over 10^3 years (~ 350 binary periods P_{bin}) for prograde orbits, and over 10^4 years (~ 3500 P_{bin}) for retrograde orbits. The initial orbits were *aligned*, and both secondaries fixed in their apoastrons with respect to the primary. These integrations confirmed the theoretical stability limit $\rho \sim 0.25 \equiv 0.64$ au for prograde orbits in (Holman & Wiegert 1999). For the retrograde case, the stability limit was found much larger, indeed, $\rho \sim 0.479$ (1.22 au), in accord with the formal best-fit error in (Ramm et al. 2009). However, for their model configuration stable over 10 Myr, we may calculate $a_p \sim \rho_0 \times a_{\text{bin}} / (1 + e_p) \approx 0.86$ au, where $\rho_0 = 0.379$, $a_{\text{bin}} \sim 2.55$ au, and $e_p = 0.123$. It means that the osculating semi-major axis a_p was fixed significantly different from the formal solution in Ramm et al. (2009).

4.1 Analysis of planetary orbits aligned with the binary

To extend the results of Eberle & Cuntz (2010) and Quarles et al. (2012), we applied the dynamical maps approach. We aim to illustrate the global structure of the phase space, as well as to identify possible resonances and sources of the strong instability observed in this system. As the stability indicator we use the MEGNO again. We modified our serial software to integrate the equations of motions and the variational equations of the planetary problem, in the form of a *Mechanic* module called the CSM¹. A strongly interacting planetary system with many collisional orbits requires an appropriate integrator. Hence, instead of a fixed step-size symplectic scheme, we applied the Bulirsch-Stoer-Gragg integrator implemented in the ODEX routine (Hairer et al. 1993). It provides a very good accuracy and performance (see also, e.g., Chambers 1999). The total integration time of a single initial condition was not less than 10^4 periods of the binary, and in some cases more than 3×10^5 periods. This is typically one–two orders of magnitude longer than in the direct numerical integrations by Eberle & Cuntz (2010). The time-scale is long enough to detect most significant mean motion resonances (Goździewski et al. 2008).

In the first experiment, we fixed all angles and planetary elements as in (Eberle & Cuntz 2010), and mass of the primary to $1.4 M_\odot$, $\mu = 0.28$ as in their Fig. 2. Then we computed MEGNO

maps in high-resolution 1440×900 pixels integrated over 25,000 periods of the binary. The results are illustrated in the left panel of Fig. 2 in the semi-major axis a_p — relative inclination i_{rel} -plane. This experiment confirms that the stability limit with respect to a_p is extended for retrograde orbits. For the prograde configurations, the stability limit $a_p \sim 0.6$ au is slightly smaller from the border found in the previous papers. For retrograde orbits, it is almost doubled and reaches ~ 1.2 au. A putative planet could be located at a border of this zone, filled with unstable low-order MMRs. A stable retrograde orbit found by Eberle & Cuntz (2010) lies in a region spanned by strong 4:1, 3:1, 5:2 and 2:1 MMRs. Overlapping of these resonances and their sub-resonances creates a global chaotic zone. This effect is identified as the main source of instability of planets in compact binaries (Mudryk & Wu 2006). It is also clear that finding a stable orbit at a sparse, equidistant grid around $a_p \sim 1.2$ au can be done basically by chance, see also the bottom-right panel of Fig. 4.

Configurations with intermediate mutual inclinations, roughly between $\sim 40^\circ$ and $\sim 140^\circ$, and particularly solutions close to polar orbits ($i_{\text{rel}} \sim 90^\circ$) are very chaotic. They are associated with the Kozai rezonance (Kozai 1962). For non-coplanar orbits, a border of stable zone may be much smaller than 0.4 au. Even for a hypothetical, low-mass secondary, see the right panel of Fig. 2, polar orbits are very unstable. In this case, stable prograde solutions may be found up to the stability border close to 1.2 au. We also note that individual unstable MMRs are much wider in the case of prograde orbits than in the retrograde configurations. Moreover, a close-up of the area of retrograde orbits in Fig. 3 reveal a complex net of stable and unstable motions, recalling the Arnold web shown in the bottom panels of Fig. 1. The centre of the left panel in Fig. 3 covers the 5:2 mean motion resonance. The right panel of Fig. 3 shows the MEGNO map in the same area, but with much lower resolution of 200×50 pixels, computed over 10^4 periods of the binary. We see that a fine resolution 1440×900 pixels, as well as longer integration time $\sim 3 \times 10^4$ P_{bin} are crucial to discover these fine details of the phase space.

4.2 Developing the instability

An identification of the origin of instabilities is not straightforward, because due to overlapping MMRs, a complex pattern of stable and unstable motions appears (Fig. 2 and Fig. 3). To study, how the unstable zones are developed with increasing perturbation parameter, we performed the next experiment, in which the perturber mass was gradually increased from an artificial value of $14 m_{\text{Jup}}$ (see the right panel in Fig. 2) up to the nominal value of $532 m_{\text{Jup}}$. In this way, we follow the simpler dynamical model given through Hamiltonian Eq. 1. The dynamics of the binary system is also governed by conservative Hamiltonian, hence it should reveal the same or very similar features, depending on the perturbation parameter, which may be approximated as $\epsilon_p \sim m_S/m_P \equiv \mu$, where m_S is the mass of the secondary companion ν Oct B and m_P is the mass of the primary ν Oct A. The results are illustrated as a sequence of dynamical maps in Fig. 4. These MEGNO maps were computed over $\sim 10^4$ periods of the binary. At each panel, we labeled the lowest-order MMRs and the mass of the secondary (perturber). Each *Mechanic* run occupied 256 CPUs, and computations took, depending on initial conditions (an extent of the chaotic zone) up to a few hours of CPU time.

Already for the smallest mass ratio, corresponding to brown-dwarf mass perturber, most of the phase space is strongly chaotic (the top-left panel of Fig. 4, also the right panel in Fig. 2). In the rel-

¹ This module is still developed, but is available upon request.

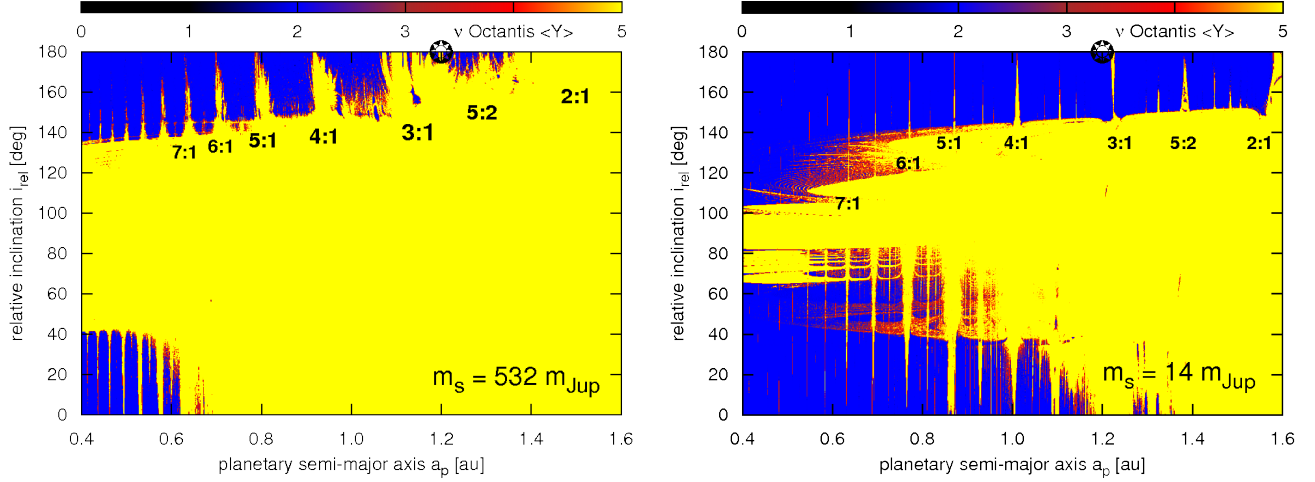


Figure 2. MEGNO dynamical maps for the geometric setup of the ν Octantis planetary system investigated by Eberle & Cuntz (2010) in which orbits of the secondary and the planet are initially aligned. A reference position of the planet in the discovery paper by Ramm et. al (2009) is marked with an asterisk. The low-order mean motion resonances between the planet and the secondary are labeled. *The left panel* is for the nominal mass of the secondary, *the right panel* is for a system with the secondary mass set to artificial value of $14 m_{\text{Jup}}$. The raw resolution of these maps is 1440×900 pixels computed for $\sim 3 \times 10^4$ periods of the binary.

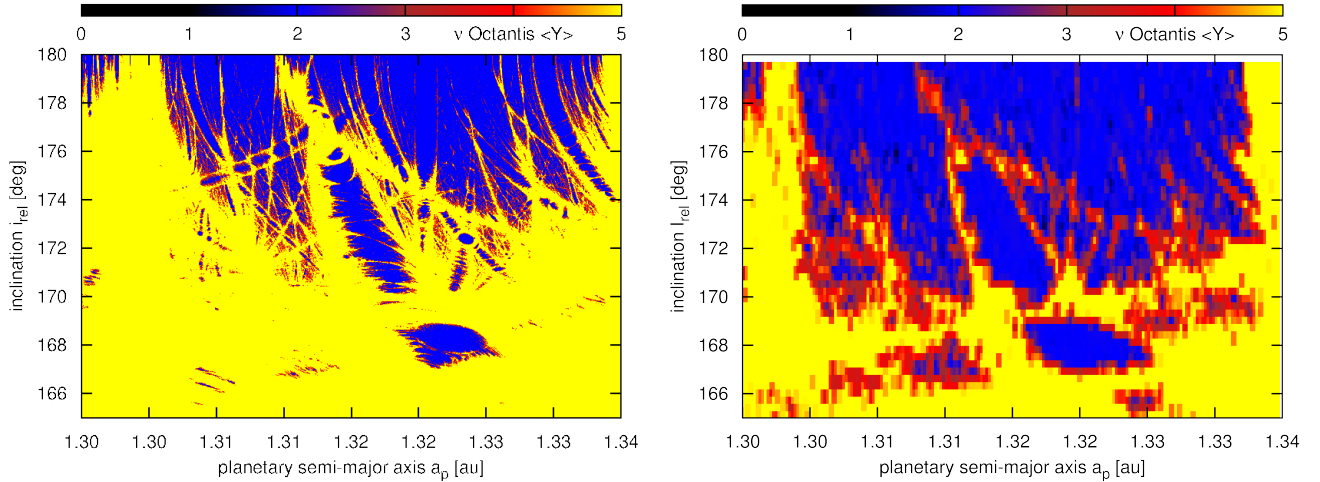


Figure 3. A close up of the MEGNO dynamical map for the orbital configuration of initially aligned orbits, in a neighborhood of the formal best-fit model in (Ramm et al. 2009). The resolution of *the left panel* is 1440×900 pixels and, for a reference, *the right panel* has 200×50 pixels. Each point was integrated over $\sim 3 \times 10^4$ and $\sim 10^4$ periods of the binary, respectively.

evant zone of retrograde orbits, a pattern of narrow MMRs appears. A retrograde orbit might have much stable space to explore than a direct orbit. In this regime, the probability of stable orbit would be close to 1. However, when the perturber mass is increased, the widths of MMRs quickly expand, and already for $m_s \sim 380 m_{\text{Jup}}$ (roughly, the left mass limit of the secondary) one may observe strong MMRs overlapping. This phenomenon emerges a zone of global chaos, roughly beyond $a_p \sim 1.2$ au. For the nominal mass of the perturber (see the bottom right panel in Fig. 4), there are left only narrow areas of stable motions.

A close-up of that region shown in Fig. 3 recalls the view of the phase space of the test Hamiltonian Eq. 1 for large values of perturbation parameter ϵ . The fine structures seen in this map represents the Arnold web in the three body problem. Although this feature is expected and has been proved in the Outer Solar system

dynamics (Guzzo 2005), likely it has not been shown in the three body problem with so much details.

From the general point of view, the dynamical stability of planetary orbits in systems with strong mutual interactions can be influenced by small changes of the initial conditions due to the presence of unstable resonances and their overlapping. However, if the mutual perturbations are small enough, and chaotic motions appear on a regular net, they may be practically stable over very long times (Guzzo 2005). Such a state of the system is called the Nekhoroshev regime. Otherwise, if the chaotic motions does not constitute a regular web, and most of orbits form a global chaotic zone, the stability of the system is influenced by a strong chaotic diffusion. This regime is related to the resonance overlapping, and is called the Chirikov regime (Froeschlé et al. 2000; Guzzo 2005).

The Arnold web emerging due to three-body MMRs was investigated by Guzzo (2005, 2006) in the Outer Solar system. He

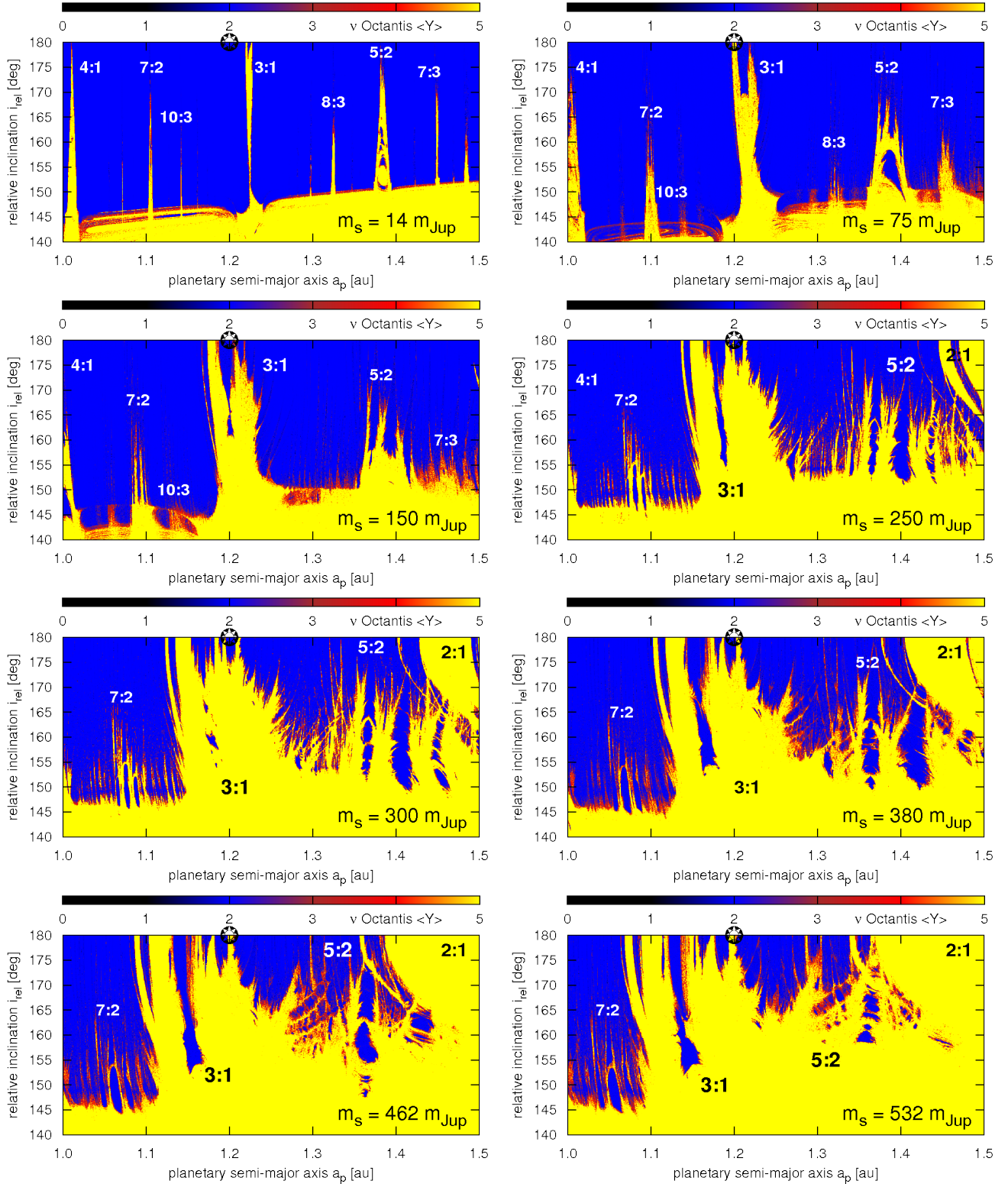


Figure 4. The results of a numerical experiment in which the secondary mass was gradually increased from the minimal value of 14 m_{Jup} (the top left panel), through 75 m_{Jup} , 150 m_{Jup} , 250 m_{Jup} , 300 m_{Jup} , 380 m_{Jup} , 462 m_{Jup} , up to the nominal mass of 532 m_{Jup} (the bottom right panel). Initial geometric configuration is fixed the same as in the retrograde orbit model by Eberle & Cuntz (2010). A reference position of the planet is marked with an asterisk. Most significant mean motion resonances between the planet and secondary are labeled. Dynamical MEGNO maps were computed over 10^4 periods of the binary.

mapped the phase space in the semi-major axes planes of Jupiter, Saturn, Uranus and Neptune. Here, we found this feature in the three-body problem in the semi-major axis — inclination plane, corresponding to a different choice of the canonical actions, and due to two-body MMRs. The Arnold web creates an intermediate zone between the ordered and strongly chaotic motions, which spans relatively large range of the inclination, extending over 10° . In this intermediate region, the phase-space motions which are chaotic, may persist over long periods of time. The results of this experiment also show that the stability limits derived numerically for co-planar binaries by Holman & Wiegert (1999) may be strongly affected by the non-coplanarity. In our case of moderate eccentricity of the planetary orbit, these limits are roughly valid for $i_{\text{rel}} \in (0^\circ, 40^\circ)$ and $i_{\text{rel}} \in (140^\circ, 180^\circ)$. Determination of the stability limits in systems with non-zero mutual inclinations needs a further, extensive numerical study, because our computations concern a particular initial configuration of the orbits. We postpone this to a new work.

4.3 The secular dynamics of the planet

The origin of a wide strip of unstable motions around polar orbits can be explained with the help of the secular octupole-level theory (e.g., Migaszewski & Goździewski 2011, and references therein). For a direct comparison with the MEGNO integrations, we focus on the initial orbital setup in (Eberle & Cuntz 2010). For small $a_p \sim 0.6$ au and less, the expansion parameter $\alpha = a_p/a_{\text{bin}} \sim 0.25$ and the system may be considered as non-resonant. This permit to study the long-term dynamics through the secular theory. The range of $a_p \in [0.4, 1.2]$ au is investigated, although α becomes as large as 0.5 at the right border of this interval. For such large values of α , the assumptions of the secular theory may be questionable.

The results are illustrated in Fig. 5 in the form of dynamical maps in the (a_p, i_{rel}) -plane. The left column is for an artificial, low-mass secondary of $14 m_{\text{Jup}}$, the right column is for the nominal mass of ν Oct B. The top row illustrates the maximal eccentricity attained by the planet over the secular orbital period. Both perturbers are massive enough to force extreme eccentricity ~ 1 . This must imply collisions with the primaries. Indeed, in the middle panels showing the maximum apocenter distance of the planet, the filled dots mark initial conditions that led to a collision with the star. These two zones closely coincide. Besides, if the initial semi-major axis is increased, the minimum distance of the planet to the secondary becomes almost always close to 0 au (see the bottom row in Fig. 5). Filled dots in these panels mark regions, in which angle $\Delta\varpi \equiv \omega_p - \omega_s$ librates. This is only possible for small mutual inclinations implying a qualitative difference of the dynamics between direct and retrograde orbits.

This experiment reveals that a continuous unstable zone between $i_{\text{rel}} \in (40^\circ, 140^\circ)$ predicted by the secular model closely coincides with unstable region around the polar orbits exhibited in the full three-body system. It means that this unstable region appear due to the Kozai resonance which force large eccentricities in the secular time-scale. Hence the primary source of instability can be identified with a *secular effect* rather than with short-term chaotic dynamics associated with the MMRs. Outside unstable zones of the Kozai resonance, the primary source of instability are the MMRs which appear as discrete areas of chaos for small value of the perturbation parameters, and a zone of global chaos when the perturbation becomes sufficiently strong and the short-term MMRs may govern the dynamics.

4.4 Newtonian model with stability constraints

To improve the Keplerian model, we conducted a search for stable configurations in terms of the N -body problem imposing stability constraints (GAMP algorithm, Goździewski et al. 2008). In this approach, unstable models are “penalized” by an artificial, large value of $(\chi_v^2)^{1/2}$ (or an rms) in course of the optimization process. The fit model allowed the mass m_{bin} , semi-major axis a_{bin} , eccentricity e_{bin} , pericenter argument ω_{bin} , inclination i_{bin} and initial mean anomaly M_{bin} of the binary to vary within the formal 3σ error bounds, in accord with the RV/astrometric Hipparchos solution in Ramm et al. (2009). The nodal longitude of the binary was fixed, $\Omega_{\text{bin}} = 87^\circ$. Error of this element is essentially irrelevant for the dynamics of the system, as it constitutes a choice of the x -axis of the coordinate frame. Mass of the planet m_p , its inclination i_p , the nodal longitude Ω_p and the remaining orbital elements with the RV offset were added to the set of 14 free parameters of the model. Standard uncertainties of the measurements in (Ramm et al. 2009) were rescaled by the “jitter” variance $\sim 5 \text{ ms}^{-1}$ in quadrature, to account for the intrinsic stellar RV variability. However, this estimate might be considered rather conservative for an active primary star. We also note, that the available Hipparchos and earlier collected astrometric data were not modeled in our code and we only used the RV measurements in (Ramm et al. 2009).

The results are shown in Fig. 6. The quality of the fits is expressed by an rms, and the solutions are marked by symbols in accord with prescribed rms bounds labeled in the panels. Filled, red circles mark regular best-fit configurations which have the MEGNO signature ~ 2 over $2000 P_{\text{bin}}$. This relatively short integration period requires an acceptable CPU-overhead, still providing at least 10-100 longer Lagrange stability time.

The statistics in Fig. 6 reveals that the best-fit configurations obtained for the mathematical N -body model cannot be well constrained. This problem concerns all orbital parameters, and in particular the eccentricity and inclination. If the rms is bounded to $\sim 22 \text{ ms}^{-1}$, similar to the best-fit Keplerian models, these elements may be varied between 0–0.6 and over 100° , respectively. The best-fit Newtonian models have an rms $\sim 20 \text{ ms}^{-1}$ for $a_p \sim 1.6$ au. These solutions correspond to one of two minima $(\chi_v^2)^{1/2}$ which can be identified in the Keplerian model. These fits are very unstable.

Dynamically stable solutions derived through the GAMP algorithm are marked with red filled circles up to an rms $\sim 25 \text{ ms}^{-1}$. Curiously, we found such stable solutions *only* as retrograde orbits, in accord with the hypothesis in (Eberle & Cuntz 2010). However, stable configurations are initially almost exactly *anti-aligned* with the binary orbit, in contrary to the *aligned* configurations in their orbital setup.

To compare the quality of these two families of models, Figure 7 displays the RV residuals of two selected best-fit models, derived without stability constraints (the top panel), and the best fit GAMP stable model (the bottom panel). In both these cases, the residuals exhibit large magnitude $120\text{--}150 \text{ ms}^{-1}$, comparable with the semi-amplitude of the RV signal $\sim 100 \text{ ms}^{-1}$ due to the putative planet itself. This large variability cannot be explained by the 1-planet model, and it may indicate strong stellar activity mimicking the planetary signal.

4.5 Stability of the GAMP model

To illustrate the dynamical neighborhood of the best-fit GAMP models, we selected a configuration with osculating elements at the epoch of the first observation in (Ramm et al. 2009) which are given

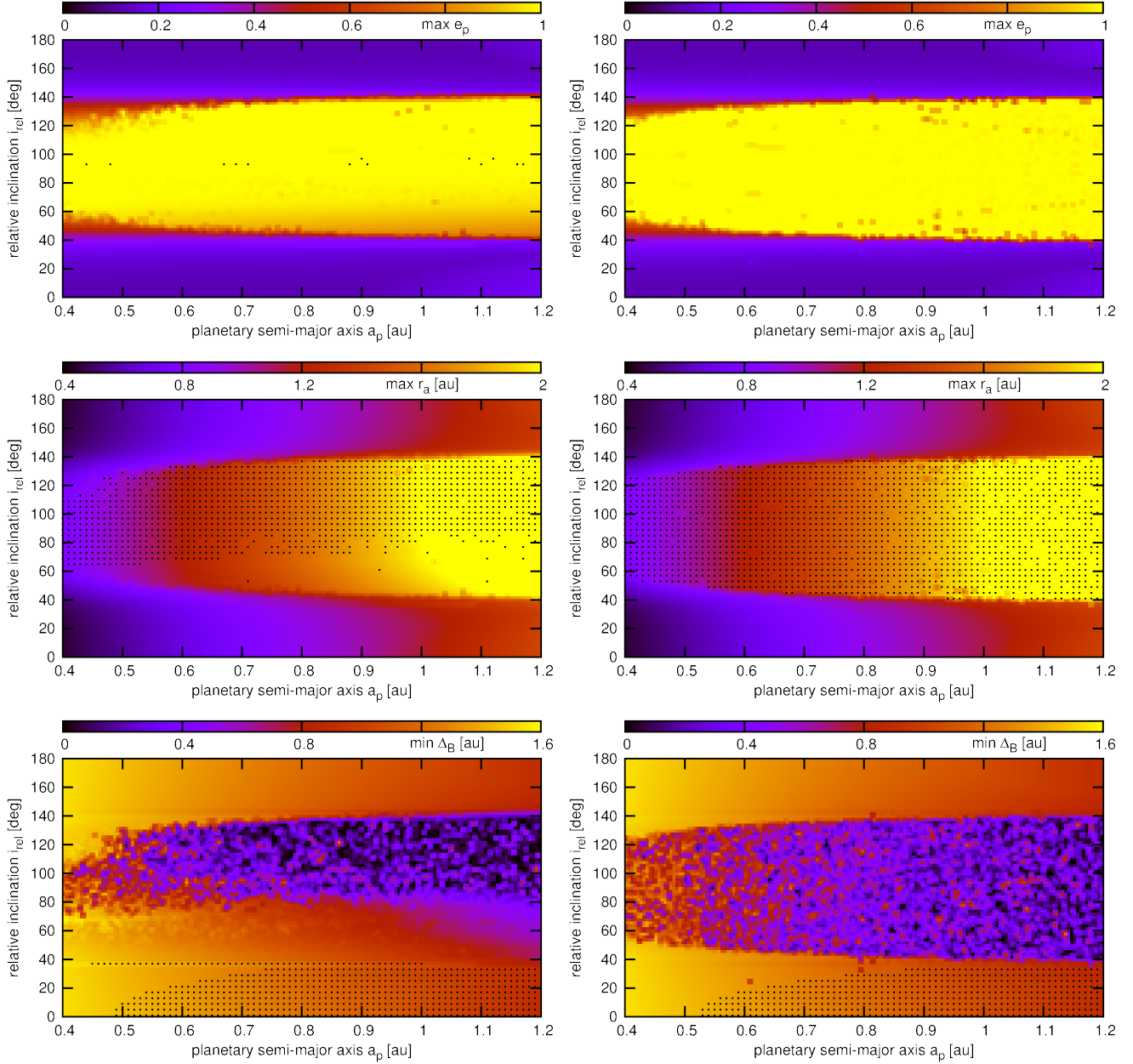


Figure 5. The orbital evolution of the secular system in terms of the octupole-level expansion w.r.t. $\alpha = a_p/a_{\text{bin}}$. The *left column* is for the secondary mass $m_B = 14 m_{\text{Jup}}$, the *right column* is for the nominal secondary $m_B = 532 m_{\text{Jup}}$. Initial geometric elements are fixed to keep $\Delta\varpi \equiv \omega_p - \omega_S = 0^\circ$ in the Laplace reference frame (aligned orbits). The *top row* is for the maximum eccentricity of the planet, the *middle row* is for the maximum of the apocenter distance of the planet and the *bottom row* is the minimum distance of the planet from the perturber. Dotted areas mark librations of $\Delta\varpi$ in the top panels, collisional orbits with the primary in the middle panels, and librations of $\Delta\varpi$ in the bottom panels.

in caption to Fig. 8. We quoted many digits, to reproduce elements of this fit possibly exactly, due to its complex and chaotic neighborhood. The formal errors may be estimated graphically in Fig. 6. Mass of the primary is fixed as $1.4 M_\odot$. An rms of this solution is $\sim 25 \text{ ms}^{-1}$.

The top-left panel of Fig. 8 illustrates the MEGNO dynamical map in the (a_p, i_p) -plane. This map shows a global view of the phase space. Note that inclination i_p is *absolute w.r.t. the astrometric frame*, in which the binary inclination is $i_{\text{bin}} \sim 71^\circ$.

Integration time for the global map is $10^4 P_{\text{bin}}$. Subsequent close-ups shown in remaining panels of Fig. 8 and in Fig. 9 were

integrated for $2 \times 10^4 P_{\text{bin}}$ up to $10^5 P_{\text{bin}}$ per each point, depending on the magnification factor. To detect weak MMRs and sub-resonances, such an extension of the integration time is indispensable. The resolution of these maps is 1440×900 pixels. Calculations were performed with the help of the Mechanic environment on the UV SGI supercomputer chimera of the Poznań Supercomputing Centre (Poland). This machine has 2048 CPU cores, and the runs spanning up to 24 hrs occupied all available hardware resources. Technically, we did not observed any bottlenecks in the master-worker inter-communication. This nice performance of the Mechanic code was expected thanks to a small overhead of the

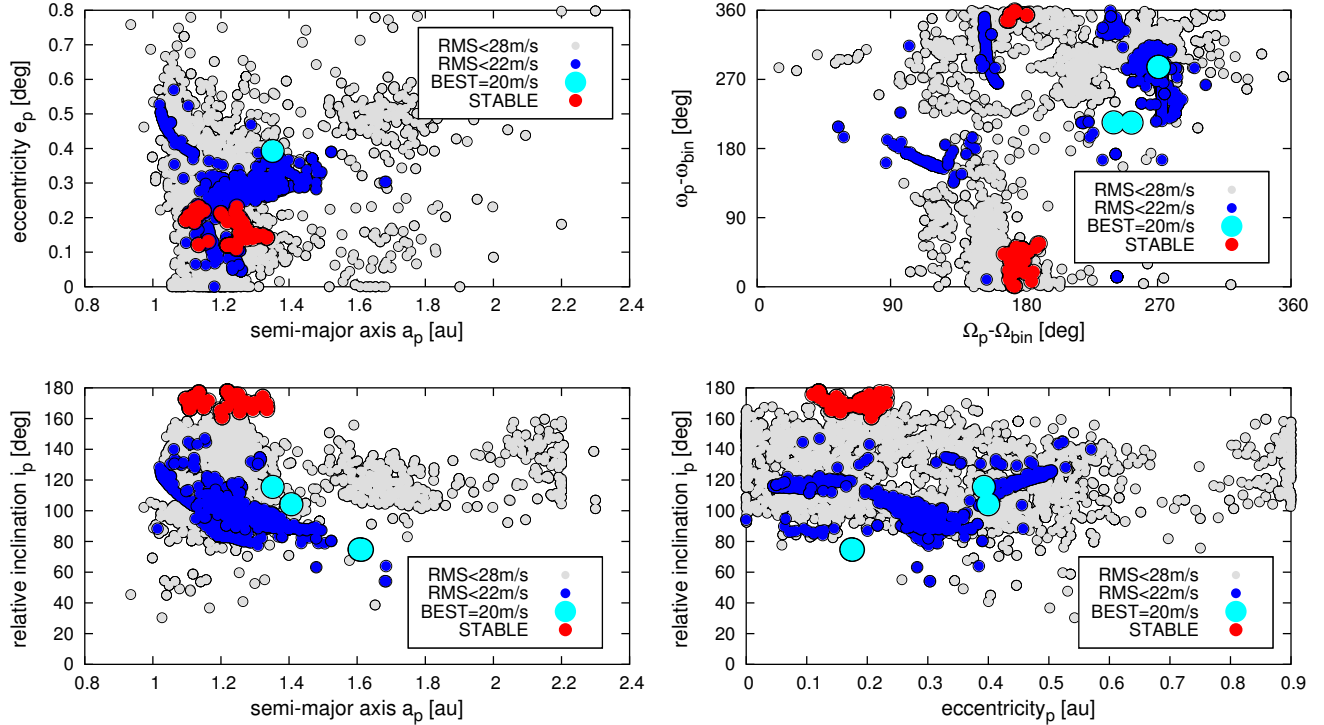


Figure 6. Statistics of the N -body and GAMP best-fit models projected onto planes of orbital osculating elements at the epoch of the first observation in (Ramm et. al 2009), gathered in the hybrid search. An rms quality of these solutions is marked with filled circles and labeled in the plots. Configurations found with imposed stability constraints, and detected as stable by the GAMP algorithm, are marked with filled red circles.

MPI data broadcasts. These computations validated the software and its ability of stable long-runs on a few thousands of CPU cores.

The global map in the top-left panel of Fig. 8 reveals that the phase space is mostly strongly chaotic. The best-fit configuration is found in a narrow stability island associated with the 7:2 MMR. For a reference, other significant MMRs are labeled in this panel. A close-up of this map shown in the top-right panel of Fig. 8 unveils an extremely complex structure of this regular island. It spans a small region covering $\Delta a_p \sim 0.02$ au and $\Delta i_p \sim 20^\circ$. In this small island, the phase space has again a sophisticated, fractal-like structure of the Arnold web.

To reveal the Arnold web in more detail, we computed a number of close-ups of this area, which are illustrated in the middle and the bottom row panels of Fig. 8 and in Fig. 9. These maps uncover weak sub-resonances, which form a regular net at any magnification level. These structures, particularly well seen in the bottom-right panel of Fig. 8 closely resemble the Arnold web of the model Hamiltonian, Eq. 1. Likely, it has been never illustrated with such a sharpness and details.

We also tested other solutions in the GAMP set, and the results are similar. The best-fit models, which obey reasonably well the observational constrains, are confined to very narrow stability islands.

5 CONCLUSIONS

We confirm a hypothesis of stable retrograde orbit in (Eberle & Cuntz 2010). However, the observational constrains require such orbits initially *anti-aligned* with the binary orbit. Besides, long-term stable solutions may be found only in narrow islands of regu-

lar, quasi-periodic motions exhibiting a complex structure of the Arnold web. It remains uncertain how a Jovian planet could be trapped in such tiny stable regions, or how it could be formed in globally unstable dynamical environment. Besides, the RV signal is very noisy, and the best-fit models reveal a large scatter of residuals having amplitude comparable with the RV signal itself. Therefore, the presence of Jovian planet in orbit around ν Oct A is still questionable. New observations are required to confirm or withdraw that explanation of the observed RV residual signal.

An efficient analysis of the observations of extrasolar planetary systems is a challenging problem. This involves not only different observational techniques and data sources, but also orbital optimization algorithms, combined with analytical and numerical stability studies. Despite the theoretical background, in most cases we usually need much computing power to perform massive numerical experiments.

In this work, we present the *Mechanic* environment, an MPI-based, Open Source task management system which helped us to perform high-resolution dynamical mapping of the phase space with the fast indicator MEGNO. *Mechanic* may become a new, general helper tool in a wide range of applications in the field of the dynamical astronomy. This framework is directed toward numerical analysis of large sets of initial conditions, like the long-term integrations of the equations of motion. We work on other applications, like quasi-global optimization with the Genetic Algorithms of different observational models of the extrasolar planetary systems. The *Mechanic* aims to be a host software framework with dedicated setup, task preparation and data storage model. It offers a consistent user API, making it possible to reuse existing serial software without significant and deep modifications. The *Mechanic* code with detailed technical documentation and sample modules

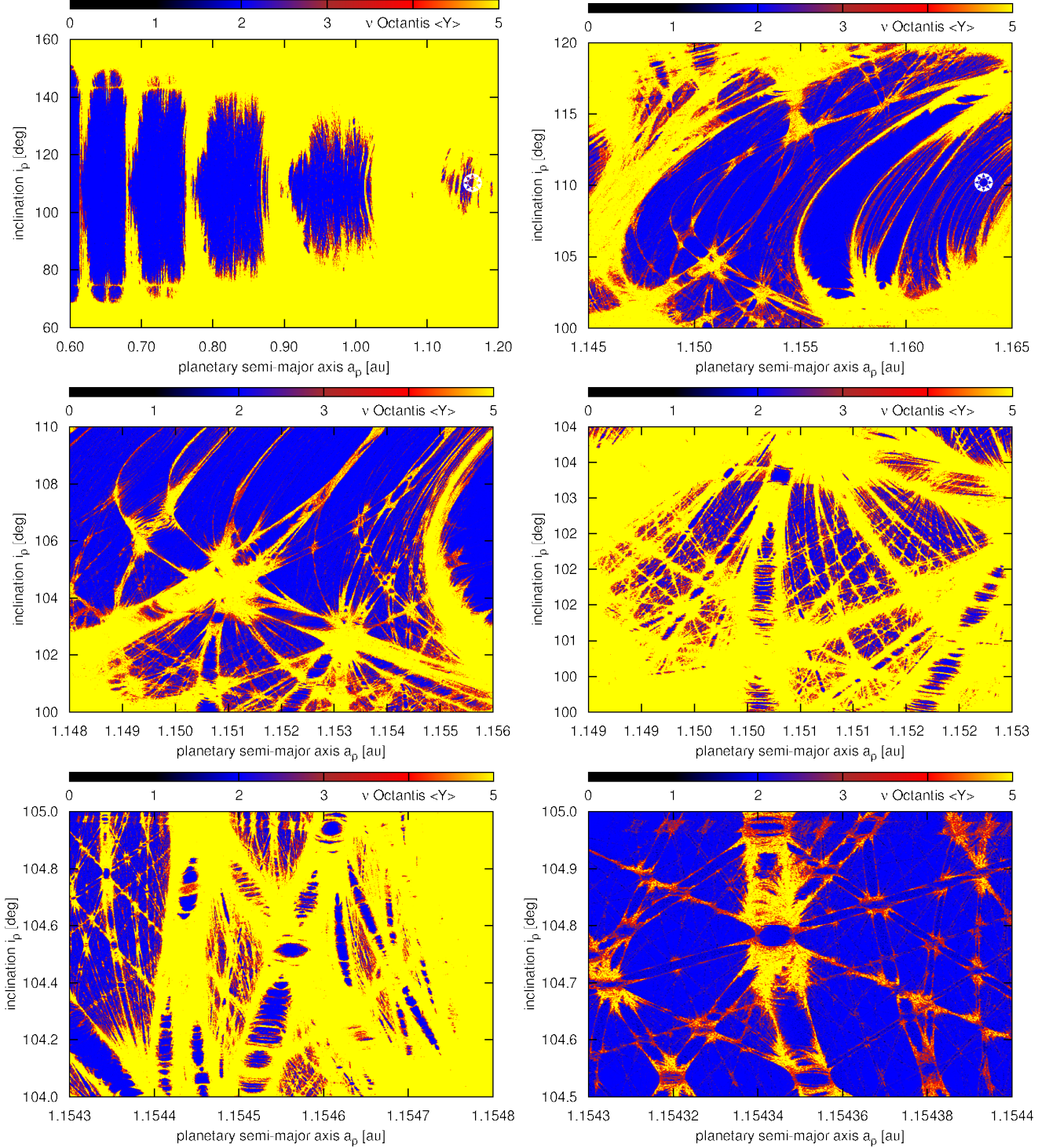


Figure 8. Dynamical maps of the best-fit stable solution found in the GAMP search in the (a_p, i_p) -plane. The top left panel is for the global view of the phase space, the top right map is for stability island of the solution. The next maps are subsequent close-ups of the neighborhood of the best-fit solution. Osculating, *astrometric* elements of the planet at the first epoch in (Ramm et. al 2009) are $m_p = 1.92596 m_{Jup}$, $a_p = 1.16365$ au, $e_p = 0.13139$, $i_p = 110.21102^\circ$, $\Omega_p = 262.29811^\circ$, $\omega_p = 127.26299^\circ$, mean anomaly $M_p = 133.16327^\circ$, respectively. Elements of the secondary are $m_s = 560.62366 m_{Jup}$, $a_{bin} = 2.52813$ au, $e_{bin} = 0.23881$, $i_{bin} = 71.28090^\circ$, $\Omega_{bin} = 87.0^\circ$, $\omega_{bin} = 74.59137^\circ$, $M_s = 339.762973^\circ$, respectively. The nominal elements of the best-fit stable model are marked with the star symbol.

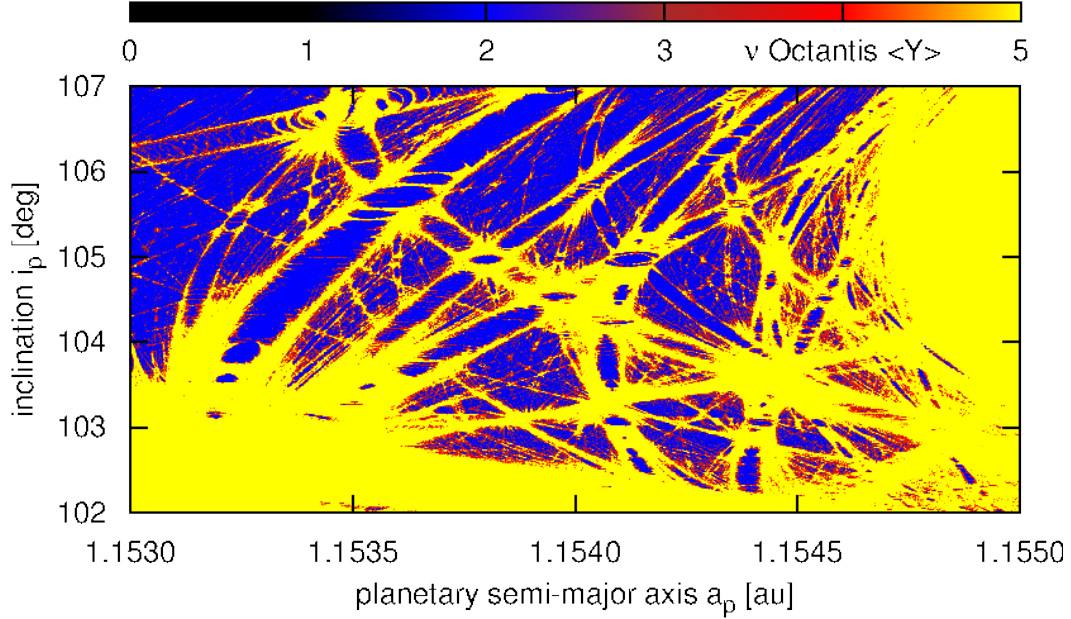


Figure 9. A close-up of the stability island of the best-fit, stable GAMP model illustrate in Fig. 8. The resolution is 1440×900 pixels. Integration time per pixel is $3 \times 10^5 P_{\text{bin}}$.

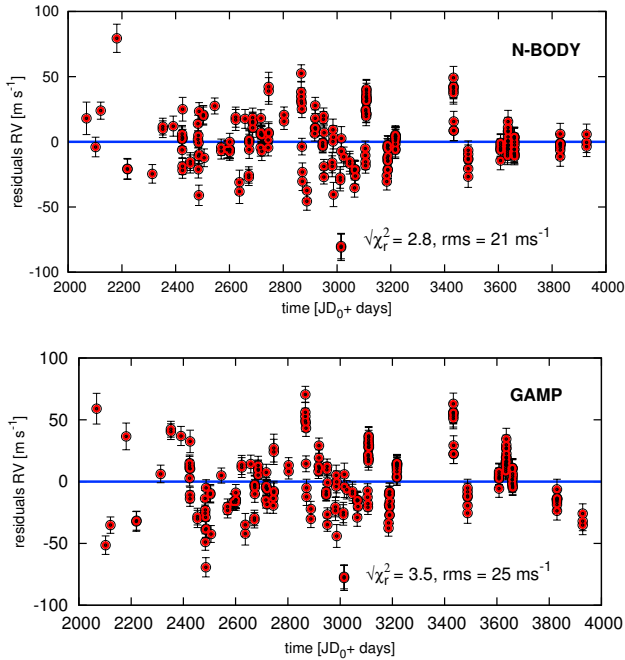


Figure 7. Residuals to representative *N*-body best fit models illustrated in Fig. 8. *The top panel* is for the formal, mathematical solution. *The bottom panel* is for the stable, GAMP-derived model.

is freely available at the project website (Słonina & Goździewski 2012). We encourage the interested readers to use it and to take a part in the development of the code and computing modules.

At present, a new concept version of *Mechanic2* is developed actively. In this new branch we aim to introduce new features and improve the functionality with a simultaneous simplification of the API.

6 ACKNOWLEDGMENTS

This work is supported by the Polish Ministry of Science and Higher Education through grant N/N203/402739. Computational part of the work is conducted within the POWIEW project supported by the European Regional Development Fund in Innovative Economy Programme POIG.02.03.00-00-018/08.

We would like to thank Tobias Hinse and Sean Delaney for their grateful tests of the *Mechanic* on several CPU-clusters, and Kacper Kowalik for valuable suggestions and help in development of the code.

APPENDIX A: OVERVIEW OF THE *Mechanic* PACKAGE

A1 The *Mechanic*

The aim of the *Mechanic* is to help in automated and consistent task preparation, distribution, check-pointing and data management, as well as data post-processing. For this reason our software differs significantly from other task management systems in terms of usage of user-supplied numerical code, that would be distributed over the computing pool. Instead of using its binary executable, we provide the Application Programming Interface (API) to connect it transparently to the communication and storage layer. Such *core—module* approach followed in the design of the *Mechanic* allows not only to run exactly the same code both in single- and multi-CPU environments, but also to unify data management. From this point of view, the *Mechanic* is a host software framework, which may help to reduce the overall code developing time and allows to reuse existing “serial” software without extensive nor structural modifications.

Since the communication layer of the *Mechanic* is developed on top of the MPI framework, the core software works on the same way on dedicated CPU-clusters, PC-workstations or laptops. It uses the *task farm* communication pattern, which introduces *master—worker* relationships between CPUs in a computing pool and helps

in splitting the workload automatically. Although the Mechanic's API hides to the end-user the MPI logic, the additional inter-node communication is possible. In such a case, a basic knowledge on parallel programming is required. The storage layer is developed on top of the well-documented self-describing HDF5 data format. This allows the output data to be reused in number of different software applications.

The Mechanic may be used system-wide, with and without control of the queue systems. The code development is performed on Linux and Mac OS platforms, however, by design it safely runs on any modern UNIX-like operating systems.

A2 Implementation of the Mechanic module

A Mechanic module is a *C-interopable* code (i.e. C++, OpenCL, Nvidia CUDA or partially Fortran2003+) compiled to a shared library. The minimal module implementation should define the basic storage layout, and task processing routine. In the language of the Mechanic the *task* may be either a call to a standalone "serial" software inside the task loop, or — a call to its numerical part, with all configuration and storage performed within the API. Tasks are assigned to workers according to the *task farm* model. The size of the task pool may be governed through the API. In case of dynamical maps, the module will use the default, two-dimensional task mapping, with initial conditions (pixels of the map) being prepared according to the coordinates of the tasks.

Let us present a minimal working module example, that computes the Arnold web (see also a listing of the coded, provided in Appendix A3).

The `arnoldweb_init()`² function, called very early during module initialisation, is used to setup all run-specific information, such as basic storage layout. Each worker node uses the input data of length `input_length` to prepare the initial condition for the task. The master node receives the output of length `output_length` and stores it in the master datafile³. In our example, we would like to prepare six state variables of the Hamiltonian (1) and receive the coordinates of the point of the map and the dynamical state of the system (the MEGNO indicator).

The preparation of the task takes place during call to `arnoldweb_task_prepare()`. Coordinates of the task are used to change the initial state of the system, so that we can obtain a dynamical map. The task is computed then in the `arnoldweb_task_process` function. We pass the initial state to the external code computing the MEGNO, and at the end of the computations, we assign the result. It is received then by the master node and stored in a HDF5 dataset. After that, the worker takes the next task (point of the map), if available.

The module code should be compiled to a shared library and placed somewhere in the library search path⁴:

```
mpicc -std=c99 mechanic_module_arnoldweb.c
-o libmechanic_module_arnoldweb.so
```

To use the module with the Mechanic one can try:

```
mpiexec -n 24 mechanic -p arnoldweb -x 512 -y 512 -d 1024
```

This will tell the Mechanic to use 24 CPU (compiting nodes) in the

default, task farm mode, for the simulation with 512×512 task pool resolution and checkpoint performed each 1024 computed tasks (pixels). The output HDF5 files may be post-processed then with helper tools that come with the package.

The source code of the Arnold web module with detailed API documentation, as well as other examples, is available at the project website (Slonina & Goździewski 2012). We would like to stress, that the user API is a subject of development, and it may change, however it presents the key concepts of the Mechanic.

A3 The Arnold web module code

```
#include "mechanic.h"

/* Implements module_init() */
int arnoldweb_init(int mpi_size, int node,
    TaskInfo *i, TaskConfig *c) {

    /* Input and output data arrays length */
    i->input_length = 6;
    i->output_length = 3;

    return MECHANIC_TASK_SUCCESS;
}

/* Implements module_task_prepare() */
int arnoldweb_task_prepare(int node, TaskInfo *i,
    TaskConfig *c, TaskData *in, TaskData *out) {
    double xmin, xmax, ymin, ymax, stepx, stepy;

    xmin = 0.8; xmax = 1.2;
    ymin = 0.8; ymax = 1.2;

    in->data[0] = 0.131; // Phi1
    in->data[1] = 0.132; // Phi2
    in->data[2] = 0.212; // Phi3

    /*
    Map coordinates:
    out->coords[0] -- x-coord
    out->coords[1] -- y-coord
    out->coords[2] -- task number
    */

    stepx = (xmax-xmin)/(1.0*c->xres);
    stepy = (ymax-ymin)/(1.0*c->yres);

    /* Modify initial state according to
    the current task */
    in->data[3] = xmin + out->coords[0]*stepx; // I1
    in->data[4] = ymin + out->coords[1]*stepy; // I2
    in->data[5] = 0.01; // I3

    return MECHANIC_TASK_SUCCESS;
}

/* Implements module_task_process() */
int arnoldweb_task_process(int node, TaskInfo *i,
    TaskConfig *c, TaskData *in, TaskData *out) {
    double xv[6], tend, step, eps, result;

    /* Integrator setup */
    step = 0.5*(sqrt(5)-1)/2; tend = 5000.0;
    eps = 0.001;

    /* Initial data */
    xv[0] = in->data[0]; xv[1] = in->data[1];
```

² API functions must be prefixed with the name of the module, *arnoldweb* here.

³ At the time of writing, data arrays are one-dimensional of type double

⁴ LD_LIBRARY_PATH for Linux and DYLIB_LIBRARY_PATH for Mac OS

```

xv[2] = in->data[2]; xv[3] = in->data[3];
xv[4] = in->data[4]; xv[5] = in->data[5];

/* The numerical procedure goes here */
result = smegno(xv, step, tend, eps);

/* Assign the master result that is suitable for
the dynamical map */
out->data[0] = xv[3]; // I1
out->data[1] = xv[4]; // I2
out->data[2] = result; // MEGNO

return MECHANIC_TASK_SUCCESS;
}

```

REFERENCES

- Adams F. C., Laughlin G., 2003, *Icarus*, 163, 290
- Alden H. L., 1939, *AJ*, 48, 81
- Arnold V. I., 1964, *Doklady Akad. Nauk SSSR* (in Russian), 5, 581
- Arnold V. I., 1978, *Mathematical methods of classical mechanics*
- Baluev R. V., 2011, *Celestial Mechanics and Dynamical Astronomy*, 111, 235
- Barrio R., Borczyk W., Breiter S., 2009, *Chaos Solitons and Fractals*, 40, 1697
- Chambers J. E., 1999, *MNRAS*, 304, 793
- Cincotta P. M., 2002, *New Astronomy*, 46, 13
- Cincotta P. M., Giordano C. M., Simó C., 2003, *Physica D Non-linear Phenomena*, 182, 151
- Cincotta P. M., Simó C., 2000, *A&A*, 147, 205
- Colacevich A., 1935, *PASP*, 47, 87
- Dvorak R., 1984, *Celestial Mechanics*, 34, 369
- Eberle J., Cuntz M., 2010, *ApJL*, 721, L168
- Fields S., , 1993, *Hunting For Wasted Computing Power. New Software for Computing Networks Puts Idle PC's to Work*
- Froeschlé C., Guzzo M., Lega E., 2000, *Science*, 289, 2108
- Froeschlé C., Lega E., Gonczi R., 1997, *Celestial Mechanics and Dynamical Astronomy*, 67, 41
- Goździewski K., Breiter S., Borczyk W., 2008, *MNRAS*, 383, 989
- Goździewski K., Konacki M., Maciejewski A. J., 2003, *ApJ*, 594, 1019
- Goździewski K., Konacki M., Wolszczan A., 2005, *ApJ*, 619, 1084
- Guzzo M., 2005, *Icarus*, 174, 273
- Guzzo M., 2006, *Icarus*, 181, 475
- Hairer E., Norsett S. P., Wanner G., 1993, *Solving Ordinary Differential Equations I. Nonstiff Problems*. Springer Verlag
- Holman M. J., Wiegert P. A., 1999, *AJ*, 117, 621
- Kley W., 2010, in K. Goździewski, A. Niedzielski, & J. Schneider ed., *EAS Publications Series Vol. 42 of EAS Publications Series, The formation of massive planets in binary star systems*. pp 227–238
- Kozai Y., 1962, *AJ*, 67, 591
- Laskar J., 1993, *Celestial Mechanics and Dynamical Astronomy*, 56, 191
- Laskar J., Robutel P., 2001, *Celestial Mechanics and Dynamical Astronomy*, 80, 39
- Lega E., Guzzo M., Froeschlé C., 2003, *Physica D Nonlinear Phenomena*, 182, 179
- Mestre M. F., Cincotta P. M., Giordano C. M., 2011, *MNRAS*, 414, L100
- Michtchenko T. A., Ferraz-Mello S., 2001, *AJ*, 122, 474
- Migaszewski C., Goździewski K., 2011, *MNRAS*, 411, 565
- Mikkola S., Innanen K., 1999, *Celestial Mechanics and Dynamical Astronomy*, 74, 59
- Morais M. H. M., Correia A. C. M., 2012, *MNRAS*, 419, 3447
- Mudryk L. R., Wu Y., 2006, *ApJ*, 639, 423
- Pacheco P., 1996, *Parallel Programming with MPI*. Morgan Kaufmann
- Quarles B., Cuntz M., Musielak Z. E., 2012, *MNRAS*
- Ramm D. J., Pourbaix D., Hearnshaw J. B., Komonjinda S., 2009, *MNRAS*, 394, 1695
- Robutel P., Laskar J., 2001, *Icarus*, 152, 4
- Sidlichovský M., Nesvorný D., 1996, *Celestial Mechanics and Dynamical Astronomy*, 65, 137
- Słonina M., Goździewski K., , 2012, *The Mechanic User Guide*, <http://www.git.astri.umk.pl/project/mechanic>
- The HDF5 Group, 2012, *Hierarchical Data Format*, <http://www.hdfgroup.org>
- Wisdom J., 1983, *Icarus*, 56, 51
- Yu L., Moretti C., Thrasher A., Emrich S., Judd K., Thain D., 2010, *Cluster Computing*, 13, 243